

Microbially-Induced Soil Colloidal Phosphorus Mobilization Under Anoxic Conditions

Kamel M. Eltohamy ^{a,b}, Daniel Menezes-Blackburn ^c, Erwin Klumpp ^d, Chunlong Liu ^e, Junwei Jin ^a, Chaogang Xing ^f, Yuanyuan Lu ^a, Xinqiang Liang ^{a,e*}

^a *Key Laboratory of Environment Remediation and Ecological Health, Ministry of Education, College of Environmental and Resource Sciences, Zhejiang University, Hangzhou 310058, China*

^b *Department of Water Relations & Field Irrigation, National Research Centre, Dokki, Cairo 12622, Egypt*

^c *Department of Soils, Water and Agricultural Engineering, Sultan Qaboos University, PO Box 34, Al-Khoud 123, Sultanate of Oman*

^d *Institute of Bio- and Geosciences, Agrosphere (IBG-3), Forschungszentrum Jülich GmbH, Jülich 52425, Germany*

^e *Key Laboratory of Mollisols Agroecology, Northeast Institute of Geography and Agroecology, Chinese Academy of Sciences, Harbin 150081, China*

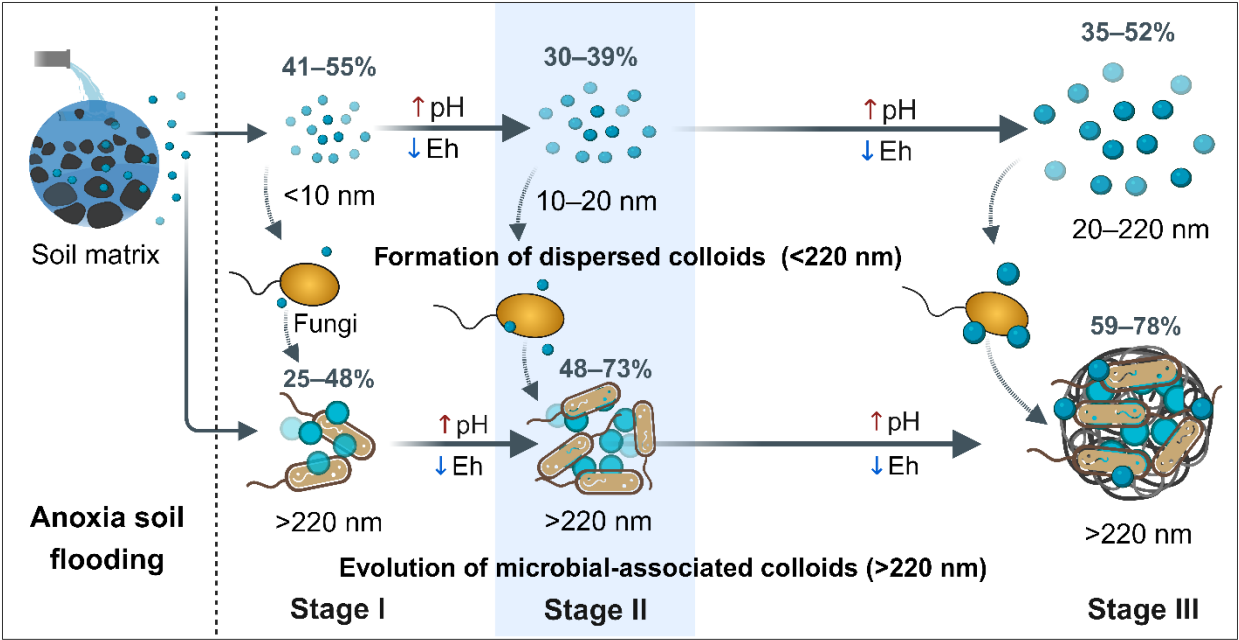
^f *Analysis Center of Agrobiological Sciences of Zhejiang University, Hangzhou 310058, China*

* Corresponding author: Xin-qiang Liang, e-mail: liang410@zju.edu.cn; Tel: 86-571-88982809

ABSTRACT: Understanding the behavior of colloidal phosphorus (P_{coll}) under anoxic conditions is pivotal for addressing soil phosphorus (P) mobilization and transport, and its impact on nutrient cycling. Our study investigated P_{coll} dynamics in an acidic floodplain soil during a 30-day flooding event. The sudden oxic-to-anoxic shift led to a significant rise in pore-water P_{coll} levels, which exceeded soluble P levels by more than 2.7-fold. Colloidal fractions transitioned from dispersed forms (<220 nm) to colloid-associated microaggregates (>220 nm), as confirmed by electron microscopy. The observed increase in colloidal sizes was paralleled by their heightened ability to form aggregates. Compared to sterile control conditions, anoxia prompted the transformation of initially dispersed colloids into larger particles through microbial activity. Curiously, the 16S rRNA and ITS microbial diversity analysis indicated that fungi were more strongly associated with anoxia-induced colloidal release than bacteria. These microbially induced shifts in P_{coll} lead to its higher mobility and transport, with direct implications for P release from soil into floodwaters.

KEYWORDS: *Floodplain soils, Colloidal phosphorus, Microbe-associated colloids, Phosphorus Mobilization, Anoxic Conditions*

SYNOPSIS: Anoxic flooding induces shifts in colloidal fractions, transitioning from dispersed (<220 nm) to >220 nm microaggregates, mediated by microbes, notably fungi, enhancing phosphorus mobility in floodplain soils.



■ INTRODUCTION

Soil flooding is a natural phenomenon that exerts a profound impact on biogeochemical processes and nutrient cycling in terrestrial ecosystems.^{1–3} The occurrence of prolonged flooding alters redox conditions, significantly affecting the availability of nutrients, particularly phosphorus (P) and its associated colloids.^{4,5} These anoxic conditions, induced by prolonged flooding, often lead to an enhanced release of P and its subsequent loss to surface water bodies.⁶ This is primarily due to favored reductive dissolution reactions, in which iron (Fe) and manganese (Mn) oxides are solubilized, and P associated with them is released into the soil pore water.^{7,8} Additionally, changes in soil pH resulting from flooding may further contribute to enhanced P release.⁹ Once P is released into soil pore water, colloidal particles, capable of settling yet remaining suspended for extended periods,¹⁰ transport this P to adjacent water bodies,^{11,12} constituting a non-point source of pollution.^{13,14} Recent studies have highlighted the association of elevated P concentrations in soil pore water, streams, and various aquatic environments with colloidal particles.^{15–20} Hence, understanding the behavior of colloidal phosphorus (P_{coll}) and associated components under anoxic conditions is critical for an accurate risk assessment of P loss in floodplain soils.

The P_{coll} is recognized as a particularly mobile form of P,^{3,21} contributing significantly to P loss from agricultural systems^{22,23} and eutrophication of freshwater bodies.^{24,25} It constitutes a substantial portion of total P in agricultural systems (13%–95%)^{3,26} and streams (up to 30%).^{18,27} Soil P_{coll} mobility is influenced by various physical, chemical, and biological factors,^{28,29} with pH, organic carbon (OC) and elements such as Fe, aluminum (Al), Mn, and calcium (Ca) being significant.^{10,30} Despite its known importance, P_{coll} behavior under reducing (anoxic) conditions is under-researched. A prior study on grassland soils revealed the anoxia-induced release of colloid- and nanoparticle-bound P <450 nm, influenced by Fe.⁵ Yet, the microbial community's role,

including bacterial membrane precipitates during colloidal bacteria transport, remains overlooked. Reports suggest that these bacterial membrane precipitates can likewise be mobile, especially during advective flow.^{31,32} Thus, further investigations are needed to comprehend the implications of microbial involvement in P_{coll} and mobility, particularly in floodplain soils.

During soil flooding, the shift to anoxic conditions decreases soil redox potential (Eh) and alters pH, affecting the biogeochemistry of redox-sensitive elements like Fe, Mn, and associated P.^{5,33} This transition also triggers a change in the microbial community, favoring anaerobic respiration-capable microorganisms.^{4,34} Microbially mediated reductive dissolution of Fe and Mn oxides, releasing P, is well-documented in flooded soils.^{4,33} Microorganisms select alternative electron acceptors like Fe^{3+} and Mn^{4+} to facilitate their metabolic processes, with the choice guided by the acceptors' energy yield and availability.^{31,34,35} For instance, in soils rich in Fe^{3+} hydroxides, microorganisms employ Fe^{3+} as the terminal electron acceptor,^{31,36} leading to the reduction of Fe^{3+} to Fe^{2+} and consequent substantial release of associated P.^{5,37}

Apart from microbial processes, dispersed colloids (<220 nm) have also a crucial role in P mobility and transport.^{11,15} Two mechanisms govern their behavior in non-anoxic soil pore water: diffusion of P-carrying nanoparticles (<20 nm) and fine colloids (20–220 nm), and modulation of soil P-desorption kinetics.¹⁵ Meanwhile, Henderson et al.⁵ linked the dispersion of P-enriched particles during anoxic conditions to biogeochemical processes that accumulate Fe and P in the >3 kDa fraction. Yet, the occurrence and formation of these dispersed colloids under anoxia remain relatively unexplored. Their development is likely intertwined with microbial activity and redox processes, contributing to P_{coll} mobilization and release under these conditions.

Given these insights, we hypothesize that anoxia promotes the formation and evolution of microbe-associated colloids (>220 nm), acting as a dynamic pool for soil P_{coll} retention and release.

We further postulate that microbe-associated colloids evolve mainly through incremental growth on microbial templates, starting from dispersed colloids (<220 nm). These dispersed colloids, in turn, predominantly arise from soil matrix-associated nanoparticles and soluble species, all influenced by anoxic biogeochemical processes. Our specific objectives are: (i) To unravel the effects of prolonged soil flooding on P_{coll} dynamics and its role in P mobilization in acidic soil; (ii) To examine the microbial communities and processes associated with the release of soil colloids after a sudden anoxic shift; and (iii) To explore the formation mechanisms of dispersed colloidal fractions under anoxic conditions.

■ MATERIALS AND METHODS

Study Site and Soil Sampling. Topsoil (0–20 cm depth) was sampled from a flood-prone paddy field in Ling Xi, Zhejiang, China (coordinates 27.5155° N, 120.3577° E). Ling Xi has a subtropical monsoon climate with annual averages, including a temperature of 17.9°C and 1769 mm of rainfall.

A composite soil sample was taken from three distinct areas within the field, totaling 30 kg. Post-collection procedures involved air-drying the soil, sieving it to a 2-mm granularity, and storing it at a controlled temperature of $25 \pm 1^\circ\text{C}$. Additional geographical, climate specifics, and initial soil characteristics are described in Supplementary Information (SI) Section 1 and Table S1.

Microcosm Design and Flooding Experiments. Soil flooding tests were carried out with a set of microcosms, conforming to previously established methodologies.^{31,38} For each microcosm, 450 g of air-dry soil was equilibrated with 1.5 L of artificial river water—containing 0.6 mM each of NaCl and CaSO_4 , along with 0.3 mM of $\text{Mg}(\text{NO}_3)_2$ —to closely simulate the characteristic composition of river water during flooding events.^{31,38} This step was essential for ensuring the ecological validity of our flooding simulations. This soil-water mixture was agitated on an end-

over-end shaker (Thermo Scientific Labquake, United States) for 2 h at room conditions.³¹ Following spinning at 600×g for 15 min, the supernatant was decanted, and the residual soil paste was transferred to the microcosm and submerged in 0.5 L of synthetic river water. Twelve hours later, 10 mL of pore water was extracted from the suction cup at a flow rate of 0.4 mL min⁻¹ to exchange its dead volume.³¹ The ultimate microcosm geometry involved a water-saturated soil layer of ~9 cm height (with a pore water-to-soil ratio of 1.0 L kg⁻¹) covered by a 6 cm layer of overlying floodwater. All microcosms used polyethylene bottles (Metrohm, China) equipped with a microporous suction apparatus (10–16 µm pore size; EcoTech, Germany), positioned ~3.5 cm below the soil-water interface and connected to a Teflon valve. The performance of the suction cup was found to be superior to other materials with respect to metal sorption based on previous studies.³¹ Microcosms were incubated in a temperature-stabilized incubator (Binder KB 400, Germany; ± 0.1 °C) at a constant 25 °C for 30 days in a dark environment. Dual controls were implemented: one series included 0.04% formaldehyde (w/v) to inhibit microbial activity,³⁹ while the other was continuously aerated to sustain oxic conditions. The incubation course was determined given that the physicochemical characteristics of the submerged paddy soils typically reach apparent equilibrium within a month.²

Pore-water Sampling and Colloid Fractionation. Soil pore-water samples were systematically collected at specific intervals (days 1, 2, 3, 5, 10, 15, 20, 25, and 30) using a syringe pump, with a controlled flow rate set at 0.4 mL min⁻¹. This flow rate was intentionally chosen to minimize potential external forces' impact on soil grains.² Sampling was conducted within an anoxic glovebox (pO₂ <1 ppm; Braun, Germany). Following sampling, a portion of the solution was immediately used to measure Eh and pH using a portable pH/ORP analyzer (HACH, SENSION + pH1, United States).

Unfiltered aliquots were taken from the pore-water sample before the remainder was filtered. The filtration process utilized 0.22 and 0.025 μm cellulose-nitrate membranes (Millipore, United States); the initial 1.5 mL of the filtrate was discarded to minimize contamination. A slow syringe-drive-imposed flow rate of 0.2 mL min^{-1} (yielding a flow rate of $10^{-3} \text{ cm s}^{-1}$ across the membrane) was chosen based on recommendations for colloid size fractionation.³¹ To perform size fractionation of freely dispersed colloids, ultrafiltration was executed using disposable filtration units with distinct molecular weight cut-offs (MWCO: 10, 100, 300, and 1000 kDa; Microsep®, Pall Corp.). This filtration process was carried out on days 5, 10, and 25 via centrifugation at 3500 $\times g$ for 20 minutes.² All size-fractionation steps were performed within the glovebox.

A subset of filtered samples was acid-adjusted to a pH <2 using 1 M nitric acid, and analyzed for total P, Fe, Mn, Al, and Ca concentrations via inductively coupled plasma-mass spectrometry (ICP-MS, Agilent 7800, United States). Rhodium (^{103}Rh) served as the internal standard, sourced from the National Sharing Platform for Reference Material (GSS2). Total OC concentrations were quantified with a total OC (TOC) instrument (multi-N/C2100, Analytik Jena, Germany), post-acidification to a pH <2 using 0.5 M hydrochloric acid. Quality control measures, including the use of Certified Reference Materials (CRMs), were employed as detailed in SI Section 2 and Table S2.

Quantification of Soluble and Colloidal Concentrations. The colloidal (C_{coll}^i) and soluble (C_{aq}^i) concentrations were inferred from the concentrations measured in the unfiltered (C_{unf}^i) and the 0.025 μm -filtered ($C_{0.025\mu\text{m}}^i$) pore water aliquot according to Eqs. (1) and (2):^{2,31,40}

$$C_{\text{coll}}^i = C_{\text{unf}}^i - C_{0.025\mu\text{m}}^i \quad (1)$$

$$C_{\text{aq}}^i = C_{0.025\mu\text{m}}^i \quad (2)$$

In addition, the colloidal fractions below and above 0.22 μm (220 nm) were employed to segregate larger suspended colloidal aggregates from those in free dispersion in the pore water.² Specifically, concentration metrics for both associated ($C_{>220\text{nm}}^i$) and dispersed colloidal forms ($C_{<220\text{nm}}^i$) were inferred based on established methodologies (Eqs. (3) and (4)).

$$C_{>220\text{nm}}^i = C_{\text{unf}}^i - C_{0.22\mu\text{m}}^i \quad (3)$$

$$C_{<220\text{nm}}^i = C_{0.22\mu\text{m}}^i - C_{0.025\mu\text{m}}^i \quad (4)$$

Here, $C_{0.22\mu\text{m}}$ denotes the concentration measured in pore water filtered through a 0.22 μm pore size.

The microbially-induced colloidal release into the pore water was calculated as the difference between their concentrations in the unsterilized and formaldehyde-sterilized control under anoxic conditions for both associated ($C_{>220\text{nm}}^i$) and dispersed colloidal forms ($C_{<220\text{nm}}^i$). The microbially induced $C_{>220\text{nm}}^i$ colloidal fraction may contain microbial cells whereas the dispersed fraction may only contain microbial exudates. Namely, these were inferred based on Eqs. (5) and (6).

$$C_{>220\text{nm}-\text{microbial}}^i = C_{>220\text{nm}-\text{anoxic}}^i - C_{>220\text{nm}-\text{anoxic}-\text{sterilized}}^i \quad (5)$$

$$C_{<220\text{nm}-\text{microbial}}^i = C_{<220\text{nm}-\text{anoxic}}^i - C_{<220\text{nm}-\text{anoxic}-\text{sterilized}}^i \quad (6)$$

A negative value outcome of Eq. (6) indicates that the presence of microbes inhibited the formation of this dispersed fraction rather than induced their release in the pore water.

Pore-water Colloids Characterization. Morphological analysis of pore-water colloids was conducted using a transmission electron microscopy (TEM; JEOL 1200 EX, Tokyo, Japan) at specific time points—days 1, 5, 10, and 25. Specimens were prepared by applying 1.5 mL of unfiltered pore-water samples to TEM grids, followed by drying in a glovebox and subsequent storage under a nitrogen atmosphere until analysis.^{2,31,38} It is important to note that the drying process might lead to the formation of nanoparticle aggregates, often localized in segregated

patches at the droplet's perimeter.⁴¹ This phenomenon is attributed to surface dewetting⁴² and the 'coffee-ring' effect,⁴³ which can influence the observed size and morphology of the colloids.

Microbial Community Profiling and Data Pre-processing. Following a 30-day soil flooding experiment, soil samples (0.5 g) were taken from both anoxic and oxic microcosms ($n = 3$). The genomic DNA was extracted using Qiagen's DNeasy PowerSoil Kits and preserved at -80°C before further analysis. For the amplification of bacterial 16S rDNA genes, primers 27F (5'-AGRGTTYGATYMTGGCTCAG-3') and 1492R (5'-TASGGHTACCTTGTTASGACTT-3') were employed, whereas fungal ITS genes were targeted using primers ITS1F (5'-CTTGGTCATTTAGAGGAAGTAA-3') and ITS4R (5'-TCCTCCGCTTATTGATATGC-3').⁴⁴ The PCR protocol comprised a denaturation step at 95°C , 30 amplification cycles consisting of denaturation at 95°C for 60 s, annealing at 50°C for 60 s, and extension at 72°C for 60 seconds, and a final extension at 72°C for 7 minutes.⁴⁵ Amplification products were subjected to gel electrophoresis, processed, and integrated into a SMRTbell sequencing library for PacBio SMRT sequencing. PCR products were used to create the Illumina DNA library, and sequencing was executed on a MiSeq following the manufacturer's guidelines. Data processing and microbial diversity analyses were conducted with software the tools SMRT Link v8.0, USEARCH v.10.0, and QIIME2, utilizing databases like SILVA and UNITE. Biomarker Technologies Corporation facilitated these processes (See SI Section 3 for more details). During processing, sequences were rid of barcodes and primers, with the removal of sequences containing ambiguous base calls, as well as short sequences <150 bp. Subsequent denoising was performed, defining operational taxonomic units through clustering at 3% divergence (97% similarity), followed by the elimination of singleton sequences and chimeras. Taxonomic classification of final zOTUs (USEARCH) was achieved using BLASTn against NCBI (www.ncbi.nlm.nih.gov). Each DNA extract yielded nearly

50k sequences.

Labile P Distribution Imaging. Two-dimensional (2-D) spatial distribution of labile P was visualized using the diffusive gradient in thin films (DGT) technique. This evaluation aimed to investigate labile P patterns across soil and overlying water interfaces after a 30-day anoxia flooding, compared to the oxic and sterilized controls. For details, please refer to SI Section 4.

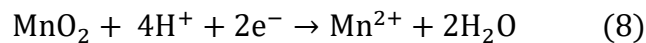
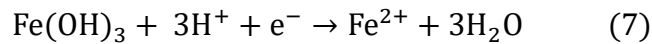
Mineralogical Analysis. The samples were air-dried in the sample chamber, ground to 300 mesh, poured into the sample holder, and then lightly pressed to ensure random orientation. Mineral phase characterization and identification of soil samples were performed using an X-ray diffractometer (XRD; Bruker D8 Advance, Germany) coupled with Jade 9.8 software and the PDF-4+ database, employing the Bragg-Brentano diffraction geometry. The scan parameters were: CuK α radiation ($\lambda = 1.5418 \text{ \AA}$) at 40 kV and 40 mA, covering an incident angle (2θ) range from 5° to 90° , with a scan step size of 0.02° and a step time of 0.2 seconds. The mineral phase content of the soil samples was quantified using the Rietveld method.⁴⁶ Following data processing in Microsoft Excel, OriginPro 2023 software (OriginLab Corp., US) was utilized for graphical representation.

Statistical Analysis. Disparities among treatments were assessed using one-way ANOVA, with validation via Tukey's test at a significance level of $p \leq 0.05$. Relationships between variables were analyzed using Pearson's correlation and further validated by t-tests, with significance and high significance set at $p \leq 0.05$ and $p \leq 0.01$, respectively. Data transformations were employed for non-normally distributed datasets. Principal component analysis (PCA) was applied to identify soil attributes impacting pore-water P_{coll} concentrations. All analyses were performed in Microsoft Excel, SPSS v22, and JMP13, with visualizations crafted in OriginPro 2023. The interactive representation of microbial diversity was facilitated by Krona,⁴⁷ and microbial diversity indices

were computed with PAST.⁴⁸ Correlation networks of OTUs with Pearson's coefficients exceeding 0.95 were constructed using Graphia 2.0, following the Markov Cluster Algorithm (MCL) with granularity at 1.2.⁴⁹

■ RESULTS AND DISCUSSION

Redox Shifts and Soluble P Release Under Anoxic vs. Oxic Soil Flooding. Flooding the soil induced a swift and statistically significant shift from oxic to anoxic reducing conditions, as evidenced by the marked decrease in pore-water Eh during the initial 10 days (Figure 1a) and a concurrent rise in pH (Figure 1b, $p < 0.01$; Table S3). Anoxic flooding also led to heightened concentrations of soluble P (P_{aq}), along with soluble forms of Fe (Fe_{aq}), Mn (Mn_{aq}), and Al (Al_{aq}) relative to oxic or sterilized conditions ($p < 0.05$; Figure S1a–d and Table S3). This increase is primarily ascribed to the microbial-mediated reductive dissolution of Fe- and Mn-oxides (Eqs. (7) and (8)),^{50–54} releasing Fe^{2+} and Mn^{2+} into the pore water,⁴⁰ ultimately promoting the release of their associated P.³³



The absence of oxygen (O_2) renders Fe and Mn as prominent electron acceptors, facilitating the release of adsorbed and occluded P (see Figure 2a).⁵⁵ Support for this mechanism is further provided by the correlation analysis, which examines the differences in concentrations between anoxic and oxic treatments (see Figure S2). The observed increase in pore-water pH (from 5.39 to 6.63; Figure 1b) can be primarily attributed to proton-consuming reactions,³³ notably including the reductive dissolution of Fe- and Mn-oxides ($r \geq 0.94$, $p < 0.001$; Figure S2).^{9,40} However, it's worth noting that even in the oxic soil, there was an increase in pH (from 5.33 to 5.62; Figure 1b),

suggesting the involvement of additional reactions in pH elevation. As a result, this increase in pH is likely one of the vital conditions facilitating the solubilization and release of adsorbed P ($r = 0.92, p < 0.001$; Figure S2).⁴ Additionally, while Al itself doesn't undergo reductive dissolution in the manner of Fe and Mn, the changes in pore-water pH resulting from Fe and Mn reductive dissolution can indirectly drive Al solubilization ($r = 0.98, p < 0.001$; see Figure 2b).⁵⁶ The Al^{3+} release into pore water is expected to act as a flocculant, enhancing the size of colloidal aggregates.

Furthermore, the notable increase in soluble Ca (Ca_{aq}) concentrations relative to the oxic conditions ($p < 0.05$; Figure S1e and Table S3) can further be linked to the reductive dissolution of Fe- and Mn-oxides ($r \geq 0.76, p < 0.001$). Typically, Ca^{2+} ions are largely bound to soil particles, limiting their solubility in pore water,⁵⁷ a phenomenon supported by data from the controls (Figure S1e). However, this limitation seems to be bypassed through the breakdown of Ca-bound P,^{33,58} a process facilitated by the reductive dissolution of these oxide minerals (see Figure 2c)—a relationship reinforced by a robust correlation (r of Ca with P = 0.86, $p < 0.001$; Figure S2). Likewise, soluble OC (OC_{aq}) levels rose significantly compared to the oxic conditions ($p < 0.05$; Figure S1f and Table S3), a proof of the accelerated soil OM decomposition under reducing conditions (see Figure 2d), which releases OC_{aq} .⁵⁵ The rise in OC_{aq} upon anoxic flooding stems primarily from the accumulation of microbial respiration byproducts like acetate and propionate.⁴⁰ The strong correlation between OC_{aq} and the Fe_{aq} and Mn_{aq} levels in the pore water ($r \geq 0.86, p < 0.001$; Figure S2) emphasizes the role of C as a microbial energy source.⁴

Colloidal Dynamics in Anoxic vs. Oxic Soil Flooding: A Redox Response. Trends in pore-water P_{coll} concentration paralleled those of its P_{aq} counterpart (Figures 1c and S1a), albeit at more than 2.7-fold higher concentrations under anoxic conditions throughout the 30-day flooding. Anoxic flooding prompted a significant rise in colloidal levels compared to the oxic conditions (p

< 0.05; Table S3), highlighting the profound effect of anoxia on their release and accumulation in pore water. The contrasting colloidal concentrations between the sterilized control and anoxic treatment groups ($p < 0.05$; Table S3) underscores the pivotal role of microbes in this colloid rise, discussed in more detail in the following section.

Under anoxia, pore-water P_{coll} concentrations exhibited a three-stage pattern: a gradual increase from day 1 to day 3 (12.29 μM to 33.79 μM ; stage I), followed by a substantial increase from day 5 to day 10 (65.65 μM to 93.98 μM ; stage II), and then a slight rise during the remaining period (96.54 μM to 100.74 μM ; stage III) (Figure 1c). Similar patterns were observed for other colloids, except for Ca_{coll} , which reached its peak concentration earlier at day 10 (1.95 mM) and subsequently declined slightly to 1.68 mM (day 30) (see Figure 1d–h). These patterns closely aligned with pore-water Eh and pH shifts (Figure 1a, b) and showed strong correlations (Eh: $r > -0.85$, pH: $r > 0.88$; $p < 0.01$), notably exceeding those with Ca_{Coll} (Eh: $r > -0.48$, pH: $r > 0.47$; Figure S3). This demonstration of a robust connection between redox conditions, pH, and colloidal mobilization during anoxic soil flooding aligns well with previous studies.^{5,59}

The observed trends in most pore-water colloids also offer crucial insights (Figure 1c–f, h): 1) The initial increase (stage I) indicates colloid dispersion resulting from flooding. Enhanced water flow tends to boost colloid mobilization, primarily driven by heightened desorption and dissolution processes acting on solid-phase-bound colloids;^{3,60} 2) The substantial increase (stage II) in concentrations coincides with a drop in Eh (Figure 1a) and an increase of pH (Figure 1b), signifying the rapid mobilization of colloids and their release from the soil matrix due to soil reduction. This could plausibly be attributed to competitive interactions between colloidal species and soil adsorption sites. The reduction process disrupts the binding of colloidal species to larger soil particles and aggregates,^{5,31} leading to their release from the soil matrix into the pore water;⁶¹

3) The slight rise in concentrations during stage III indicates a continued but slower mobilization process, possibly due to remaining colloidal species desorbing from less accessible adsorption sites or undergoing slower dissolution.

An outlier to this trend was Ca_{coll} , which peaked on day 10 and subsequently slightly declined (Figure 1g). Unlike other colloids and even its soluble counterpart (see Figure S1e), the behavior of Ca_{coll} under anoxic conditions is noteworthy. The early peak can be plausibly linked to the onset of reductive dissolution in Fe- and Mn-oxides, which triggered the release of previously associated colloidal elements like Ca_{coll} and may have even displaced them from their adsorption sites due to the increased presence of Fe(II) and Mn(II).³¹ However, as the reduction process advances, released Ca_{coll} and some liberated phosphates likely underwent precipitation, forming colloid-sized Ca-P precipitates.^{28,55} This precipitation phenomenon was likely accelerated by the elevated pH values in the pore water ($r > 0.47$, $p < 0.05$; Figure S3).⁶² Consequently, insoluble colloid-sized Ca-P formation accounts for the subsequent decline in Ca_{coll} concentration as reduction unfolds. Conversely, under oxic conditions, pore-water Ca_{coll} levels were lower (Figure 1g), remaining relatively stable from day 5 onwards, indicating enhanced Ca_{coll} attachment to soil particles⁵⁷ and resulting in reduced its levels in pore water compared to anoxic conditions.

Microbial Role on Colloidal P Formation in Anoxic Flooded Soils. Here, we validate our initial hypothesis on microbe-associated colloid evolution in anoxic soil pore water. The anoxic release of colloids into the pore water was largely inhibited in the sterilized control, evidencing the microbial induction of colloidal release. Initially, the dispersed P_{coll} fraction ($\text{P}_{<220\text{nm}}$) dominated, constituting 60%–67% of the P_{coll} (Figure 3). Yet, as hypothesized, from day 5 (stage II) onwards, the microbe-associated P_{coll} fraction ($\text{P}_{>220\text{nm}}$) asserted dominance (stage II: 58%–62% and stage III: 69%–75% of P_{coll}). This pattern parallels observations for other colloids, with a lag

for $\text{Ca}_{>220\text{nm}}$ (Figure 3). This shift highlights the growing role of microbes in the mobilization of >220 nm colloids and bound P. Conversely, O_2 presence subdued these >220 nm colloids (Figure S4), likely due to limited certain microbial populations tied to colloid release.

To evaluate the microbial role in the colloid rise, we derived their net concentrations in anoxic conditions by subtracting levels observed in sterilized conditions (namely, C_{microbe} as $C_{\text{anoxic-sterilized}}$). The microbially-induced increase in suspended colloids of size above 220 nm may involve direct binding of microbial cells, whereas the fraction size below 220 nm may only contain microbial exudates. A prominent increase in $\text{P}_{>220\text{-microbe}}$ and congruent trends for other colloids of similar size paralleled the observed for total dispersed colloids (Figure 4). These trends underscore microbial enhancement of >220 nm colloids in anoxic environments, further corroborated by notable correlations and distinct clustering of $\text{P}_{>220\text{-microbe}}$ with other colloids compared to <220 nm colloidal fraction (Figure S5). The $\text{P}_{<220\text{-microbe}}$ (unassociated with microbial cells) showed an initial increase lower than the observed for the $\text{P}_{>220\text{-microbe}}$ fraction and was progressively reduced after day 10, indicating that these may be precursors of the formation of the $\text{P}_{>220\text{-microbe}}$ fraction. Similar trends were observed for $\text{Fe}_{<220\text{-microbe}}$, $\text{Ca}_{<220\text{-microbe}}$, $\text{Al}_{<220\text{-microbe}}$ and $\text{Mn}_{<220\text{-microbe}}$, but not for $\text{OC}_{<220\text{-microbe}}$, indicating that microbially induced OC_{coll} is likely to be over 220 nm and directly associated with the microbial biomass.

To pinpoint microbial taxa driving the >220 nm colloid increase, we profiled soil microbial communities by 16S and ITS microbial diversity, at the end of the 30-day study period under anoxic and oxic conditions. Although bacterial diversity remained relatively stable, significant differences emerged in fungal communities (Table S4), especially within dominant taxa like Ascomycota (refer to SI Section 5 and Figure S6). Bacterial and fungal sequence numbers for individual OTUs were subjected to multivariate correlation network analysis (Figure S6c), in order

to highlight microbial communities responding to both oxic and anoxic conditions. Specifically, the MCL clustering of microbial communities revealed pronounced changes in community structures: Cluster 5 showed a 292% surge under anoxic conditions, representing 2.9% of the total population, while Cluster 1, the largest cluster, saw an 11% increase, equating to 5.6% of the community. Predominantly, both these clusters were fungal-dominant, underscoring fungi's potential preference for anoxic environments. Conversely, most other clusters diminished in anoxic environments, with Cluster 4 recording the steepest drop corresponding to 18.42% of the microbial community. These observations show that the microbially induced >220 nm colloidal fraction rose in anoxia, likely due to changes in fungal community structure rather than in bacteria.

TEM elucidated the evolving nature of these colloids (Figure 5). Early observations revealed a dominance of dispersed colloids (<220 nm; Figure 5a). By day 5, colloids >220 nm increased, with further expansion by day 10 (Figure 5a). While prior studies highlight rod-shaped bacteria's role in colloid formation,^{2,31} our findings distinctly point to a prominent fungal role, particularly those belonging to the Ascomycota phylum. Notably, Ascomycota are known for effective aggregation.^{63,64} For instance, Lehmann et al.⁶⁴ demonstrated that Ascomycota strains possess both high biomass density and low leucine aminopeptidase activity, factors that collectively enhance their propensity to induce aggregate formation. Our observations corroborate these findings; by day 10, we noted an amplified tendency among these larger colloids to form aggregates, a phenomenon that became more pronounced by day 25 (Figure 5a). This aggregation propensity was attenuated under oxic conditions and was absent in sterilized controls (Figure 5b, c). This morphological evolution coincided with the increase in the concentrations of P_{>220-microbe} and associated colloids (shown in Figure 4), cementing the causal connection between microbial activity and colloid release.

Formation of Dispersed Colloids in Anoxic Environments.

To elucidate the formation mechanisms of small-sized dispersed colloids (<220 nm) under anoxia, we quantified colloidal concentrations across diverse particle size ranges via a multi-step ultrafiltration procedure. Aligning with our second hypothesis positing the primary origin of these colloids from soil matrix-related nanoparticles and soluble species under anoxic influences, we observed a parallel trend among the colloidal constituents (Figure 6). Specifically, there was a progressive increase in colloid particle size, despite variations in their concentrations. Initially, colloidal particles dominated the ~3–10 nm range on day 5, shifting to ~10–20 nm by day 10, indicative of anoxia-driven growth. By day 25, significant growth into the ~20–75 nm range occurred, affirming sustained colloid aggregation under anoxia, and directly supporting our second hypothesis. Notably, oxic and sterilized controls showed less pronounced size transformations, with sub-3 nm particles more prevalent than in anoxic treatment (see Figures S7 and S8). This size shift also coincided with a change in temporal dynamics, transitioning from a dominance of these dispersed colloids to those >220 nm colloids (see Figures 2 and 3). Sterilization limited this shift, aligning with our first hypothesis of microbe-associated colloid evolution starting from nanoscale dispersed colloids (see Figure 2e).

Unlike $P_{>220\text{-microbe}}$, $P_{<220\text{nm-microbe}}$ ascended until day 10 followed by a marked decrease thereafter (Figure 4a). This was mirrored in dispersed fractions of Fe_{coll} , Mn_{coll} , and Al_{coll} (Figure 4b–d). $\text{Ca}_{<<220\text{nm-microbe}}$ started decreasing from day 5, reaching negative values by day 25 (Figure 4e). These patterns reveal that the <220 nm colloids released post-day 10 aren't microbial-driven but mainly originate from nanoparticles or soluble species within the anoxic soil matrix. Additionally, the negative trend in $\text{OC}_{<220\text{nm-microbe}}$ from day 5 (Figure 4f) suggests microbial use

of OC_{<220nm} for energy or conversion to other C forms, such as gases or biomass, possibly via microbial respiration, methanogenesis or fermentation.

The TEM data further corroborated the enduring presence of the dispersed colloids, even while the incidence of >220 nm colloids increased with their propensity to form aggregates (Figure 5a). This emphasizes anoxia's critical role as a dynamic facilitator for the dispersion and release of diverse colloidal particles from the soil matrix in the initial days after flooding. Finally, our observations resonate with prior research suggesting that soil matrix-linked nanoparticles and soluble species serve as precursors for these dispersed colloids under anoxic conditions (see Figure 2e).² Our data also corroborate two proposed mechanisms underlying the anoxic progression of dispersed P-enriched colloidal particles: the accumulation of specific metal ions, particularly Fe, owing to anoxic biogeochemical transformations; and the initiation of variegated colloidal dispersions in the soil matrix following Fe reduction.^{5,50} A notable P-Fe correlation in dispersed colloids ($r = 0.66$, $p < 0.01$) and consistent PCA clustering with similar loadings for P and Fe dispersed colloids ($P_{\text{dispersed}} = 0.44487$ and $Fe_{\text{dispersed}} = 0.44935$; Figure S5b) confirm these mechanisms.

Implications of Anoxia-Induced Colloidal P on P Mobilization. The findings of this study hold significant environmental implications, particularly concerning the behavior of P_{coll} in anoxic conditions. The augmented presence of pore-water P_{coll} (Figure 1a) in anoxic environments, predominantly within the microbe-associated fraction (refer to Figures 3 and 4) highlights the role of post-flooding microbial processes in releasing P_{coll} from soil matrix and facilitating its mobilization into pore water. The clustering of microbes via correlation network analysis and MCL algorithm showed that the shifts in the predominantly fungal taxa were linked to colloidal release during the transition from oxic to anoxic conditions (Figure S6c). This prompts inquiries about the

role of microbial fungal community shifts leading to an increased downstream transport and repercussions of P_{coll} . This heightened microbial colloid mobilization phenomenon may be ascribed to two plausible mechanisms: firstly, the heightened activity of microbes belonging within MCL clusters 1 and 5, which could be directly contributing to colloid release in anoxic conditions; alternatively, the imposition of anoxic conditions may effectively inhibit microbes belonging to other clusters, which could have previously been involved in the binding of soil colloidal aggregates. The body of evidence gathered in this manuscript suggests that the former is more likely than the latter.

Eltohamy et al.¹⁵ posited that nanoparticles and colloids of size <220 nm potentially regulate desorbable-P supply in the plant rhizosphere, while larger colloids (>220 nm) form aggregates contributing to vertical P transport to receiving waters. Our results corroborate this, showing elevated colloid formation in anoxic conditions (Figure 3) and a tendency for these colloids to aggregate, including microbe-induced forms (Figures 4 and 5a). Anoxic conditions also led to heightened labile P across the DGT sink, an *in vitro* plant rhizosphere proxy (2D- P_{DGT} ; Figure 7a), correlating with increased P_{coll} levels in pore water (Figure 2c). This suggests that anoxia enhances P mobilization and concentration in pore water, thereby increasing the flux of labile P to overlying waters, especially when compared to other soil states (Figure 7b, c). Notably, P_{DGT} may contain colloidal particles in addition to soluble forms.^{15,65,66} These colloidal particles are implicated in P absorption through (i) direct uptake along with soluble P forms⁶⁵ and (ii) enabling more efficient labile P transport due to their small size and high mobility.¹⁵ Furthermore, colloids in the solid phase could be mobilized by plant roots, acting as a third phase to augment P delivery to the DGT device.⁶⁷

Following 30 days of flooding, XRD analysis revealed notable mineralogical alterations in the soil samples under anoxic conditions compared to oxic and sterilized conditions (Figure S9). Specifically, we observed a decrease in the content of quartz, microcline, and albite in the anoxic samples relative to the sterilized and oxic samples (Table S5, and Figures S10–S12), with Figure S9 showing a corresponding decrease in the intensity of each peak, are consistent with the theory of enhanced mineral dissolution and subsequent release of more colloids and minerals.

The accumulation and proliferation of >220 nm colloids, alongside the formation of dispersed colloids, further suggest that anoxic environments can serve as reservoirs for retaining and releasing P. Understanding the fate of these colloids, their interactions with other components, and their potential to influence P availability and cycling in aquatic systems is crucial for addressing water quality concerns and managing P dynamics in natural environments. A more nuanced understanding of the underlying drivers of P mobilization and transport can guide better water resource stewardship and environmental conservation. It is important to note that these findings, while insightful for acidic soils, may not directly apply to alkaline soils where pH dynamics and P release mechanisms under flooded conditions may differ. This limitation highlights the need for further research across varying soil pH conditions to fully understand P_{coll} dynamics in flood-affected soils.

■ ASSOCIATED CONTENT

Supporting Information


The Supporting Information is available free of charge at:

It contains additional information on the extended description of the study site and soil characterization, quality control, and analytical validation, the extended description of microbial


community profiling and data pre-processing, two-dimensional distribution imaging of labile P concentration, and supplementary results on soil microbial community composition and abundance under anoxic and oxic conditions (PDF).


■ AUTHOR INFORMATION

Corresponding Author

Xinqiang Liang – Key Laboratory of Environment Remediation and Ecological Health, Ministry of Education, College of Environmental and Resource Sciences, Zhejiang University, Hangzhou 310058, China; Key Laboratory of Mollisols Agroecology, Northeast Institute of Geography and Agroecology, Chinese Academy of Sciences, Harbin 150081, China;  orcid.org/0000-0002-3521-9761; Phone: 86-0571-88982809; Email: liang410@zju.edu.cn


Authors


Kamel M. Eltohamy – Key Laboratory of Environment Remediation and Ecological Health, Ministry of Education, College of Environmental and Resource Sciences, Zhejiang University, Hangzhou 310058, China; Department of Water Relations & Field Irrigation, National Research Centre, Dokki, Cairo 12622, Egypt;  orcid.org/0000-0002-9250-0066


Daniel Menezes-Blackburn – Department of Soils, Water and Agricultural Engineering, Sultan Qaboos University, PO Box 34, Al-Khoud 123, Sultanate of Oman;  orcid.org/0000-0002-8142-9655

Erwin Klumpp – Institute of Bio- and Geosciences, Agrosphere (IBG-3), Forschungszentrum Jülich GmbH, Jülich 52425, Germany;  orcid.org/0000-0002-4810-9414

Chunlong Liu – Key Laboratory of Mollisols Agroecology, Northeast Institute of Geography
and Agroecology, Chinese Academy of Sciences, Harbin 150081, China

Junwei Jin – Key Laboratory of Environment Remediation and Ecological Health, Ministry of
Education, College of Environmental and Resource Sciences, Zhejiang University, Hangzhou
310058, China;  orcid.org/0000-0003-4693-1137

Chaogang Xing – Analysis Center of Agrobiological and Environmental Sciences of Zhejiang
University, Hangzhou 310058, China;  orcid.org/0000-0002-5664-584X

Yuanyuan Lu – Key Laboratory of Environment Remediation and Ecological Health, Ministry
of Education, College of Environmental and Resource Sciences, Zhejiang University,
Hangzhou 310058, China;  orcid.org/0000-0001-5869-9975

Data availability

The data that support the findings of this study are available from the corresponding author upon
reasonable request.

Notes

The authors declare no competing financial interests.

■ ACKNOWLEDGMENTS

We are grateful for grants from the National Natural Science Foundation of China (22076163;
42277005), and the Bingtuan Science and Technology Program (2021DB019).

■ REFERENCES

- (1) Huang, H.; Ji, X.-B.; Cheng, L.-Y.; Zhao, F.-J.; Wang, P. Free Radicals Produced from the Oxidation of Ferrous Sulfides Promote the Remobilization of Cadmium in Paddy Soils During Drainage. *Environ. Sci. Technol.* **2021**, *55* (14), 9845–9853. <https://doi.org/10.1021/acs.est.1c00576>.
- (2) Xia, B.; Qiu, H.; Knorr, K. H.; Blodau, C.; Qiu, R. Occurrence and Fate of Colloids and Colloid-Associated Metals in a Mining-Impacted Agricultural Soil upon Prolonged Flooding. *J. Hazard. Mater.* **2018**, *348* (January), 56–66. <https://doi.org/10.1016/j.jhazmat.2018.01.026>.
- (3) Eltohamy, K. M.; Liu, C.; Khan, S.; Niyungeko, C.; Jin, Y.; Hosseini, S. H.; Li, F.; Liang, X. An Internet-Based Smart Irrigation Approach for Limiting Phosphorus Release from Organic Fertilizer-Amended Paddy Soil. *J. Clean. Prod.* **2021**, *293*, 126254. <https://doi.org/10.1016/j.jclepro.2021.126254>.
- (4) Maranguit, D.; Guillaume, T.; Kuzyakov, Y. Effects of Flooding on Phosphorus and Iron Mobilization in Highly Weathered Soils under Different Land-Use Types: Short-Term Effects and Mechanisms. *CATENA* **2017**, *158*, 161–170. <https://doi.org/10.1016/j.catena.2017.06.023>.
- (5) Henderson, R.; Kabengi, N.; Mantripragada, N.; Cabrera, M.; Hassan, S.; Thompson, A. Anoxia-Induced Release of Colloid- and Nanoparticle-Bound Phosphorus in Grassland Soils. *Environ. Sci. Technol.* **2012**, *46* (21), 11727–11734. <https://doi.org/10.1021/es302395r>.

- (6) Amarawansha, G.; Kumaragamage, D.; Flaten, D.; Zvomuya, F.; Tenuta, M. Predicting Phosphorus Release from Anaerobic, Alkaline, Flooded Soils. *J. Environ. Qual.* **2016**, *45* (4), 1452–1459. <https://doi.org/10.2134/jeq2015.05.0221>.
- (7) Scalenghe, R.; Edwards, A. C.; Barberis, E.; Ajmone-Marsan, F. Release of Phosphorus under Reducing and Simulated Open Drainage Conditions from Overfertilised Soils. *Chemosphere* **2014**, *95*, 289–294. <https://doi.org/10.1016/j.chemosphere.2013.09.016>.
- (8) Obour, A. K.; Silveira, M. L.; Vendramini, J. M. B.; Sollenberger, L. E.; O'Connor, G. A. Fluctuating Water Table Effect on Phosphorus Release and Availability from a Florida Spodosol. *Nutr. Cycl. Agroecosystems* **2011**, *91* (2), 207–217. <https://doi.org/10.1007/s10705-011-9456-y>.
- (9) Jin, J.; Fang, Y.; Liu, C.; Eltohamy, K. M.; He, S.; Li, F.; Lu, Y.; Liang, X. Reduced Colloidal Phosphorus Release from Paddy Soils: A Synergistic Effect of Micro-/Nano-Sized Biochars and Intermittent Anoxic Condition. *Sci. Total Environ.* **2023**, *905*, 167104. <https://doi.org/10.1016/j.scitotenv.2023.167104>.
- (10) Eltohamy, K. M.; Milham, P. J.; Gouda, M.; Menezes-Blackburn, D.; Khan, S.; Liu, B.; Jin, J.; Ye, Y.; Liang, X. Size and Composition of Colloidal Phosphorus across Agricultural Soils Amended with Biochar, Manure and Biogas Slurry. *Carbon Res.* **2023**, *2* (1), 16. <https://doi.org/10.1007/s44246-023-00048-2>.
- (11) Li, F.; Zhang, Q.; Klumpp, E.; Bol, R.; Nischwitz, V.; Ge, Z.; Liang, X. Organic Carbon Linkage with Soil Colloidal Phosphorus at Regional and Field Scales: Insights from Size Fractionation of Fine Particles. *Environ. Sci. Technol.* **2021**, *55* (9), 5815–5825. <https://doi.org/10.1021/acs.est.0c07709>.

- (12) Liang, X.; Jin, Y.; Zhao, Y.; Wang, Z.; Yin, R.; Tian, G. Release and Migration of Colloidal Phosphorus from a Typical Agricultural Field under Long-Term Phosphorus Fertilization in Southeastern China. *J. Soils Sediments* **2016**, *16* (3), 842–853. <https://doi.org/10.1007/s11368-015-1290-4>.
- (13) Khan, S.; Milham, P. J.; Eltohamy, K. M.; Hamid, Y.; Li, F.; Jin, J.; He, M.; Liang, X. Pteris Vittata Plantation Decrease Colloidal Phosphorus Contents by Reducing Degree of Phosphorus Saturation in Manure Amended Soils. *J. Environ. Manage.* **2022**, *304* (August 2021), 114214. <https://doi.org/10.1016/j.jenvman.2021.114214>.
- (14) Wang, L.; Missong, A.; Amelung, W.; Willbold, S.; Prietzel, J.; Klumpp, E. Dissolved and Colloidal Phosphorus Affect P Cycling in Calcareous Forest Soils. *Geoderma* **2020**, *375* (June), 114507. <https://doi.org/10.1016/j.geoderma.2020.114507>.
- (15) Eltohamy, K. M.; Li, J.; Gouda, M.; Menezes-Blackburn, D.; Milham, P. J.; Khan, S.; Li, F.; Liu, C.; Xu, J.; Liang, X. Nano and Fine Colloids Suspended in the Soil Solution Regulate Phosphorus Desorption and Lability in Organic Fertiliser-Amended Soils. *Sci. Total Environ.* **2023**, *858*, 160195. <https://doi.org/10.1016/j.scitotenv.2022.160195>.
- (16) Baken, S.; Regelink, I. C.; Comans, R. N. J.; Smolders, E.; Koopmans, G. F. Iron-Rich Colloids as Carriers of Phosphorus in Streams: A Field-Flow Fractionation Study. *Water Res.* **2016**, *99*, 83–90. <https://doi.org/10.1016/j.watres.2016.04.060>.
- (17) Gottselig, N.; Sohrt, J.; Uhlig, D.; Nischwitz, V.; Weiler, M.; Amelung, W. Groundwater Controls on Colloidal Transport in Forest Stream Waters. *Sci. Total Environ.* **2020**, *717*. <https://doi.org/10.1016/j.scitotenv.2019.134638>.

- (18) Gottselig, N.; Nischwitz, V.; Meyn, T.; Amelung, W.; Bol, R.; Halle, C.; Vereecken, H.; Siemens, J.; Klumpp, E. Phosphorus Binding to Nanoparticles and Colloids in Forest Stream Waters. *Vadose Zo. J.* **2017**, *16* (3), vzj2016.07.0064. <https://doi.org/10.2136/vzj2016.07.0064>.
- (19) Liu, B.; Lu, Y.; Yang, J.; Eltohamy, K. M.; Fang, Y.; Tavakkoli, E.; Liang, X. Navigating the Complexity of Colloidal Phosphorus in Water: Sources, Occurrence, Transformations, and Eco-Friendly Removal Strategies. *Crit. Rev. Environ. Sci. Technol.* **2023**, 1–19. <https://doi.org/10.1080/10643389.2024.2317685>.
- (20) Wang, Z.; Eltohamy, K. M.; Liu, B.; Jin, J.; Liang, X. Effects of Drying-Rewetting Cycles on Colloidal Phosphorus Composition in Paddy and Vegetable Soils. *Sci. Total Environ.* **2024**, *907*, 168016. <https://doi.org/10.1016/j.scitotenv.2023.168016>.
- (21) Guo, Y.; Lu, Y.; Eltohamy, K. M.; Liu, C.; Fang, Y.; Guan, Y.; Liu, B.; Yang, J.; Liang, X. Contribution of Biogas Slurry-Derived Colloids to Plant P Uptake and Phosphatase Activities: Spatiotemporal Response. *Environ. Sci. Technol.* **2023**, *57* (43), 16564–16574. <https://doi.org/10.1021/acs.est.3c05108>.
- (22) Heathwaite, L.; Haygarth, P.; Matthews, R.; Preedy, N.; Butler, P. Evaluating Colloidal Phosphorus Delivery to Surface Waters from Diffuse Agricultural Sources. *J. Environ. Qual.* **2005**, *34* (1), 287–298. <https://doi.org/10.2134/jeq2005.0287a>.
- (23) Li, F.; Liang, X.; Li, H.; Jin, Y.; Jin, J.; He, M.; Klumpp, E.; Bol, R. Enhanced Soil Aggregate Stability Limits Colloidal Phosphorus Loss Potentials in Agricultural Systems. *Environ. Sci. Eur.* **2020**, *32* (1), 17. <https://doi.org/10.1186/s12302-020-0299-5>.
- (24) Li, F.; Jin, Y.; He, S.; Jin, J.; Wang, Z.; Khan, S.; Tian, G.; Liang, X. Use of Polyacrylamide Modified Biochar Coupled with Organic and Chemical Fertilizers for Reducing Phosphorus

- Loss under Different Cropping Systems. *Agric. Ecosyst. Environ.* **2021**, 310. <https://doi.org/10.1016/j.agee.2021.107306>.
- (25) Bol, R.; Gruau, G.; Mellander, P. E.; Dupas, R.; Bechmann, M.; Skarbøvik, E.; Bieroza, M.; Djodjic, F.; Glendell, M.; Jordan, P.; Van der Grift, B.; Rode, M.; Smolders, E.; Verbeeck, M.; Gu, S.; Klumpp, E.; Pohle, I.; Fresne, M.; Gascuel-Oudou, C. Challenges of Reducing Phosphorus Based Water Eutrophication in the Agricultural Landscapes of Northwest Europe. *Front. Mar. Sci.* **2018**, 5 (AUG), 1–16. <https://doi.org/10.3389/fmars.2018.00276>.
- (26) Wang, Z.; Chen, L.; Liu, C.; Jin, Y.; Li, F.; Khan, S.; Liang, X. Reduced Colloidal Phosphorus Loss Potential and Enhanced Phosphorus Availability by Manure-Derived Biochar Addition to Paddy Soils. *Geoderma* **2021**, 402 (July), 115348. <https://doi.org/10.1016/j.geoderma.2021.115348>.
- (27) Fresne, M.; Jordan, P.; Daly, K.; Fenton, O.; Mellander, P. E. The Role of Colloids and Other Fractions in the Below-Ground Delivery of Phosphorus from Agricultural Hillslopes to Streams. *Catena* **2022**, 208. <https://doi.org/10.1016/j.catena.2021.105735>.
- (28) Chen, A.; Arai, Y. *Current Uncertainties in Assessing the Colloidal Phosphorus Loss from Soil*, 1st ed.; Elsevier Inc., 2020; Vol. 163. <https://doi.org/10.1016/bs.agron.2020.05.002>.
- (29) Khan, S.; Liu, C.; Milham, P. J.; Eltohamy, K. M.; Hamid, Y.; Jin, J.; He, M.; Liang, X. Nano and Micro Manure Amendments Decrease Degree of Phosphorus Saturation and Colloidal Phosphorus Release from Agriculture Soils. *Sci. Total Environ.* **2022**, 845. <https://doi.org/10.1016/j.scitotenv.2022.157278>.
- (30) Eltohamy, K. M.; Khan, S.; He, S.; Li, J.; Liu, C.; Liang, X. Prediction of Nano, Fine, and Medium Colloidal Phosphorus in Agricultural Soils with Machine Learning. *Environ. Res.* **2023**, 220, 115222. <https://doi.org/10.1016/j.envres.2023.115222>.

- 599 (31) Weber, F. A.; Voegelin, A.; Kaegi, R.; Kretzschmar, R. Contaminant Mobilization by
600 Metallic Copper and Metal Sulphide Colloids in Flooded Soil. *Nat. Geosci.* **2009**, 2 (4),
601 267–271. <https://doi.org/10.1038/ngeo476>.
- 602 (32) Tufenkji, N. Modeling Microbial Transport in Porous Media: Traditional Approaches and
603 Recent Developments. *Adv. Water Resour.* **2007**, 30 (6), 1455–1469.
604 <https://doi.org/https://doi.org/10.1016/j.advwatres.2006.05.014>.
- 605 (33) Attanayake, C. P.; Kumaragamage, D.; Amarawansa, G.; Hettiarachchi, G. M.; Indraratne,
606 S. P.; Goltz, D. M. Phosphorus Release and Speciation in Manganese(IV) Oxide and
607 Zeolite-Amended Flooded Soils. *Environ. Sci. Technol.* **2022**, 56 (12), 8082–8093.
608 <https://doi.org/10.1021/acs.est.2c01185>.
- 609 (34) Unger, I. M.; Kennedy, A. C.; Muzika, R.-M. Flooding Effects on Soil Microbial
610 Communities. *Appl. Soil Ecol.* **2009**, 42 (1), 1–8.
611 <https://doi.org/https://doi.org/10.1016/j.apsoil.2009.01.007>.
- 612 (35) Loeb, R.; Lamers, L. P. M.; Roelofs, J. G. M. Prediction of Phosphorus Mobilisation in
613 Inundated Floodplain Soils. *Environ. Pollut.* **2008**, 156 (2), 325–331.
614 <https://doi.org/https://doi.org/10.1016/j.envpol.2008.02.006>.
- 615 (36) Sánchez-Alcalá, I.; del Campillo, M. C.; Torrent, J.; Straub, K. L.; Kraemer, S. M. Iron(III)
616 Reduction in Anaerobically Incubated Suspensions of Highly Calcareous Agricultural Soils.
617 *Soil Sci. Soc. Am. J.* **2011**, 75 (6), 2136–2146.
618 <https://doi.org/https://doi.org/10.2136/sssaj2011.0050>.
- 619 (37) Jiang, X.; Wulf, A.; Bol, R.; Klumpp, E. Phosphorus Content in Water Extractable Soil
620 Colloids over a 2000 Years Chronosequence of Paddy-Rice Management in the Yangtze

621 River Delta, China. *Geoderma* **2023**, 430, 116296.
622 <https://doi.org/https://doi.org/10.1016/j.geoderma.2022.116296>.

623 (38) Hofacker, A. F.; Voegelin, A.; Kaegi, R.; Kretzschmar, R. Mercury Mobilization in a
624 Flooded Soil by Incorporation into Metallic Copper and Metal Sulfide Nanoparticles.
625 *Environ. Sci. Technol.* **2013**, 47 (14), 7739–7746. <https://doi.org/10.1021/es4010976>.

626 (39) Liisa, T.; Timo, K.; Helinä, H. Comparison of Methods for Inhibiting Bacterial Activity in
627 Sediment. *Appl. Environ. Microbiol.* **1994**, 60 (9), 3454–3457.
628 <https://doi.org/10.1128/aem.60.9.3454-3457.1994>.

629 (40) Hofacker, A. F.; Voegelin, A.; Kaegi, R.; Weber, F.-A.; Kretzschmar, R. Temperature-
630 Dependent Formation of Metallic Copper and Metal Sulfide Nanoparticles during Flooding
631 of a Contaminated Soil. *Geochim. Cosmochim. Acta* **2013**, 103, 316–332.
632 <https://doi.org/https://doi.org/10.1016/j.gca.2012.10.053>.

633 (41) Michen, B.; Geers, C.; Vanhecke, D.; Endes, C.; Rothen-Rutishauser, B.; Balog, S.; Petri-
634 Fink, A. Avoiding Drying-Artifacts in Transmission Electron Microscopy: Characterizing
635 the Size and Colloidal State of Nanoparticles. *Sci. Rep.* **2015**, 5 (1), 9793.
636 <https://doi.org/10.1038/srep09793>.

637 (42) Bell, N. C.; Minelli, C.; Tompkins, J.; Stevens, M. M.; Shard, A. G. Emerging Techniques
638 for Submicrometer Particle Sizing Applied to Stöber Silica. *Langmuir* **2012**, 28 (29),
639 10860–10872. <https://doi.org/10.1021/la301351k>.

640 (43) Deegan, R. D.; Bakajin, O.; Dupont, T. F.; Huber, G.; Nagel, S. R.; Witten, T. A. Capillary
641 Flow as the Cause of Ring Stains from Dried Liquid Drops. *Nature* **1997**, 389 (6653), 827–
642 829. <https://doi.org/10.1038/39827>.

- 643 (44) Wang, X.; Eltohamy, K. M.; Liu, C.; Li, F.; Fang, Y.; Kawasaki, A.; Liang, X. Biochar
644 Reduces Colloidal Phosphorus in Soil Aggregates: The Role of Microbial Communities. *J.*
645 *Environ. Manage.* **2023**, *326*, 116745.
646 <https://doi.org/https://doi.org/10.1016/j.jenvman.2022.116745>.
- 647 (45) Shi, X.; Zhao, X.; Ren, J.; Dong, J.; Zhang, H.; Dong, Q.; Jiang, C.; Zhong, C.; Zhou, Y.;
648 Yu, H. Influence of Peanut, Sorghum, and Soil Salinity on Microbial Community
649 Composition in Interspecific Interaction Zone. *Frontiers in Microbiology*. 2021.
650 <https://www.frontiersin.org/articles/10.3389/fmicb.2021.678250>.
- 651 (46) Rietveld, H. M. A Profile Refinement Method for Nuclear and Magnetic Structures. *J. Appl.*
652 *Crystallogr.* **1969**, *2* (2), 65–71.
653 <https://doi.org/https://doi.org/10.1107/S0021889869006558>.
- 654 (47) Ondov, B. D.; Bergman, N. H.; Phillippy, A. M. Interactive Metagenomic Visualization in
655 a Web Browser. *BMC Bioinformatics* **2011**, *12* (1), 385. [https://doi.org/10.1186/1471-2105-](https://doi.org/10.1186/1471-2105-12-385)
656 [12-385](https://doi.org/10.1186/1471-2105-12-385).
- 657 (48) Hammer, Ø.; Harper, D. A. T.; Ryan, P. D. PAST: Paleontological Statistics Software
658 Package for Education and Data Analysis Version 2.09; 2001.
- 659 (49) Köhler, J.; Baumbach, J.; Taubert, J.; Specht, M.; Skusa, A.; Rüegg, A.; Rawlings, C.;
660 Verrier, P.; Philippi, S. Graph-Based Analysis and Visualization of Experimental Results
661 with ONDEX. *Bioinformatics* **2006**, *22* (11), 1383–1390.
662 <https://doi.org/10.1093/bioinformatics/btl081>.
- 663 (50) Huang, J.; Zhang, H. Redox Reactions of Iron and Manganese Oxides in Complex Systems.
664 *Front. Environ. Sci. Eng.* **2020**, *14* (5), 76. <https://doi.org/10.1007/s11783-020-1255-8>.

- 665 (51) Suter, D.; Banwart, S.; Stumm, W. Dissolution of Hydrous Iron(III) Oxides by Reductive
666 Mechanisms. *Langmuir* **1991**, 7 (4), 809–813. <https://doi.org/10.1021/la00052a033>.
- 667 (52) Buettner, S. W.; Kramer, M. G.; Chadwick, O. A.; Thompson, A. Mobilization of Colloidal
668 Carbon during Iron Reduction in Basaltic Soils. *Geoderma* **2014**, 221–222, 139–145.
669 <https://doi.org/https://doi.org/10.1016/j.geoderma.2014.01.012>.
- 670 (53) Wilson, S. C.; Lockwood, P. V; Ashley, P. M.; Tighe, M. The Chemistry and Behaviour of
671 Antimony in the Soil Environment with Comparisons to Arsenic: A Critical Review.
672 *Environ. Pollut.* **2010**, 158 (5), 1169–1181.
673 <https://doi.org/https://doi.org/10.1016/j.envpol.2009.10.045>.
- 674 (54) Yu, K. Redox Potential Control on Cumulative Global Warming Potentials from Irrigated
675 Rice Fields. In *Understanding Greenhouse Gas Emissions from Agricultural Management*;
676 ACS Symposium Series; American Chemical Society, 2011; Vol. 1072, pp 121-134 SE – 7.
677 <https://doi.org/doi:10.1021/bk-2011-1072.ch007>.
- 678 (55) Shaheen, S. M.; Wang, J.; Baumann, K.; Wang, S.-L.; Leinweber, P.; Rinklebe, J. Redox-
679 Induced Mobilization of Phosphorus in Groundwater Affected Arable Soil Profiles.
680 *Chemosphere* **2021**, 275, 129928.
681 <https://doi.org/https://doi.org/10.1016/j.chemosphere.2021.129928>.
- 682 (56) Driscoll, C. T.; Schecher, W. D. The Chemistry of Aluminum in the Environment. *Environ.*
683 *Geochem. Health* **1990**, 12 (1), 28–49. <https://doi.org/10.1007/BF01734046>.
- 684 (57) Rachmadetin, J.; Mizuto, M.; Tanaka, S.; Kozaki, T.; Watanabe, N. Calcium Carbonate
685 Precipitation in Compacted Bentonite Using Electromigration Reaction Method and Its
686 Application to Estimate the Ion Activity Coefficient in the Porewater. *J. Nucl. Sci. Technol.*
687 **2019**, 56 (11), 959–970. <https://doi.org/10.1080/00223131.2019.1630020>.

- 688 (58) Zhang, S.; Yang, X.; Hsu, L. C.; Liu, Y. T.; Wang, S. L.; White, J. R.; Shaheen, S. M.; Chen,
689 Q.; Rinklebe, J. Soil Acidification Enhances the Mobilization of Phosphorus under Anoxic
690 Conditions in an Agricultural Soil: Investigating the Potential for Loss of Phosphorus to
691 Water and the Associated Environmental Risk. *Sci. Total Environ.* **2021**, 793 (June), 148531.
692 <https://doi.org/10.1016/j.scitotenv.2021.148531>.
- 693 (59) Said-Pullicino, D.; Giannetta, B.; Demeglio, B.; Missong, A.; Gottselig, N.; Romani, M.;
694 Bol, R.; Klumpp, E.; Celi, L. Redox-Driven Changes in Water-Dispersible Colloids and
695 Their Role in Carbon Cycling in Hydromorphic Soils. *Geoderma* **2021**, 385 (December
696 2020), 114894. <https://doi.org/10.1016/j.geoderma.2020.114894>.
- 697 (60) Mohanty, S. K.; Saiers, J. E.; Ryan, J. N. Colloid Mobilization in a Fractured Soil: Effect
698 of Pore-Water Exchange between Preferential Flow Paths and Soil Matrix. *Environ. Sci.*
699 *Technol.* **2016**, 50 (5), 2310–2317. <https://doi.org/10.1021/acs.est.5b04767>.
- 700 (61) Borch, T.; Kretzschmar, R.; Kappler, A.; Cappellen, P. Van; Ginder-Vogel, M.; Voegelin,
701 A.; Campbell, K. Biogeochemical Redox Processes and Their Impact on Contaminant
702 Dynamics. *Environ. Sci. Technol.* **2010**, 44 (1), 15–23. <https://doi.org/10.1021/es9026248>.
- 703 (62) Warrinnier, R.; Bossuyt, S.; Resseguier, C.; Cambier, P.; Houot, S.; Gustafsson, J. P.; Diels,
704 J.; Smolders, E. Anaerobic Respiration in the Unsaturated Zone of Agricultural Soil
705 Mobilizes Phosphorus and Manganese. *Environ. Sci. Technol.* **2020**, 54 (8), 4922–4931.
706 <https://doi.org/10.1021/acs.est.9b06978>.
- 707 (63) Lehmann, A.; Zheng, W.; Rillig, M. C. Soil Biota Contributions to Soil Aggregation. *Nat.*
708 *Ecol. Evol.* **2017**, 1 (12), 1828–1835. <https://doi.org/10.1038/s41559-017-0344-y>.

- (64) Lehmann, A.; Zheng, W.; Ryo, M.; Soutschek, K.; Roy, J.; Rongstock, R.; Maaß, S.; Rillig, M. C. Fungal Traits Important for Soil Aggregation. *Frontiers in Microbiology*. 2020. <https://www.frontiersin.org/articles/10.3389/fmicb.2019.02904>.
- (65) Montalvo, D.; Degryse, F.; McLaughlin, M. J. Natural Colloidal P and Its Contribution to Plant P Uptake. *Environ. Sci. Technol.* **2015**, *49* (6), 3427–3434. <https://doi.org/10.1021/es504643f>.
- (66) Konrad, A.; Billiy, B.; Regenbogen, P.; Bol, R.; Lang, F.; Klumpp, E.; Siemens, J. Forest Soil Colloids Enhance Delivery of Phosphorus Into a Diffusive Gradient in Thin Films (DGT) Sink. *Front. For. Glob. Chang.* **2021**, *3* (January), 1–11. <https://doi.org/10.3389/ffgc.2020.577364>.
- (67) Menezes-Blackburn, D.; Bol, R.; Klumpp, E.; Missong, A.; Nischwitz, V.; Haygarth, P. M. Citric Acid Effect on the Abundance, Size and Composition of Water-Dispersible Soil Colloids and Its Relationship to Soil Phosphorus Desorption: A Case Study. *J. Soil Sci. Plant Nutr.* **2021**, *21* (3), 2436–2446. <https://doi.org/10.1007/s42729-021-00534-9>.

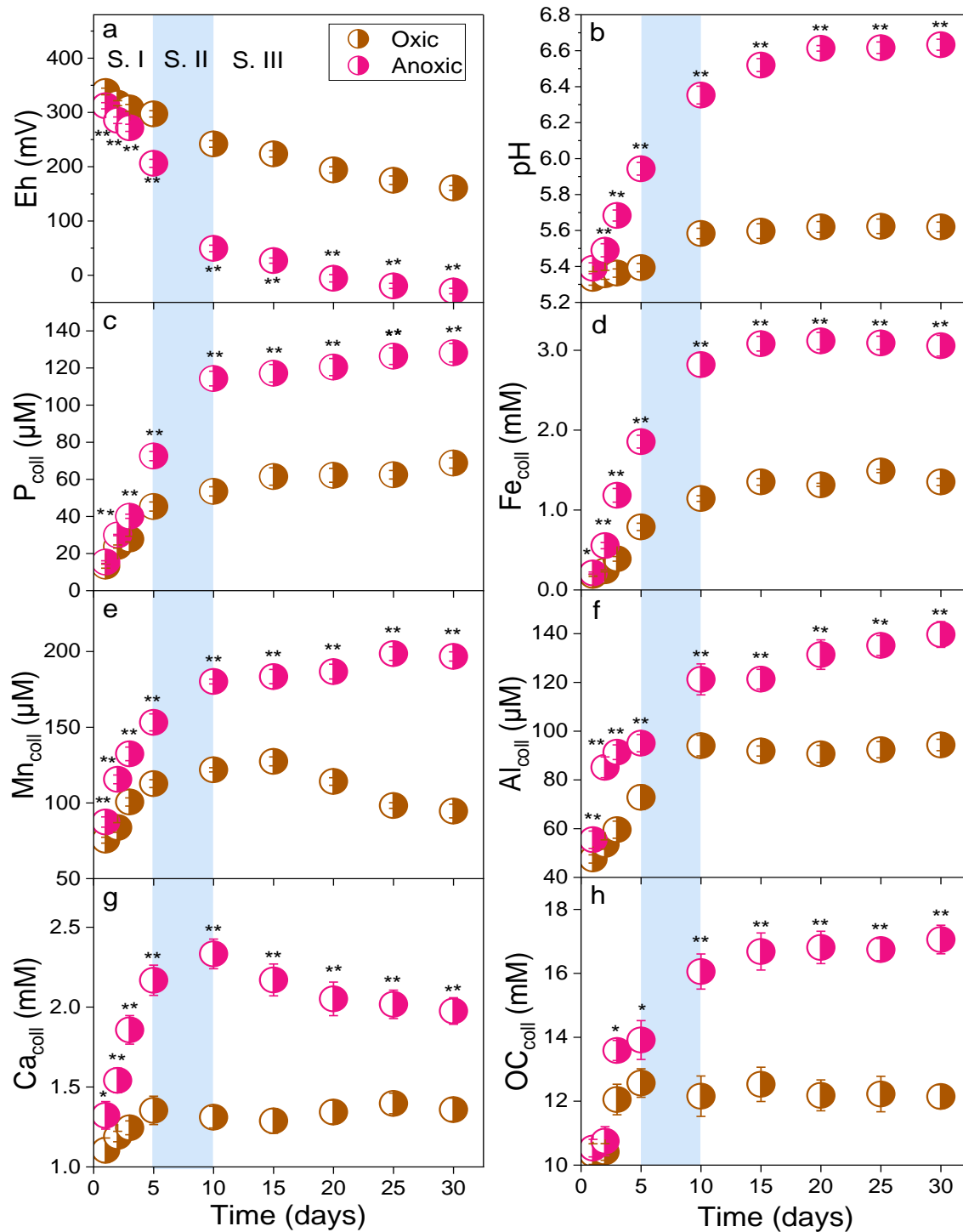


Figure 1. Temporal variations of redox potential (Eh), pH, and colloidal components (C_{coll}^i) in the soil pore water over a 30-day flooding period under anoxic and oxic conditions. Values represent means \pm SD ($n = 3$). Asterisks denote significant disparities at a given sampling time (* $p < 0.05$; ** $p < 0.01$), whereas their absence denotes no significant differences ($p < 0.05$).

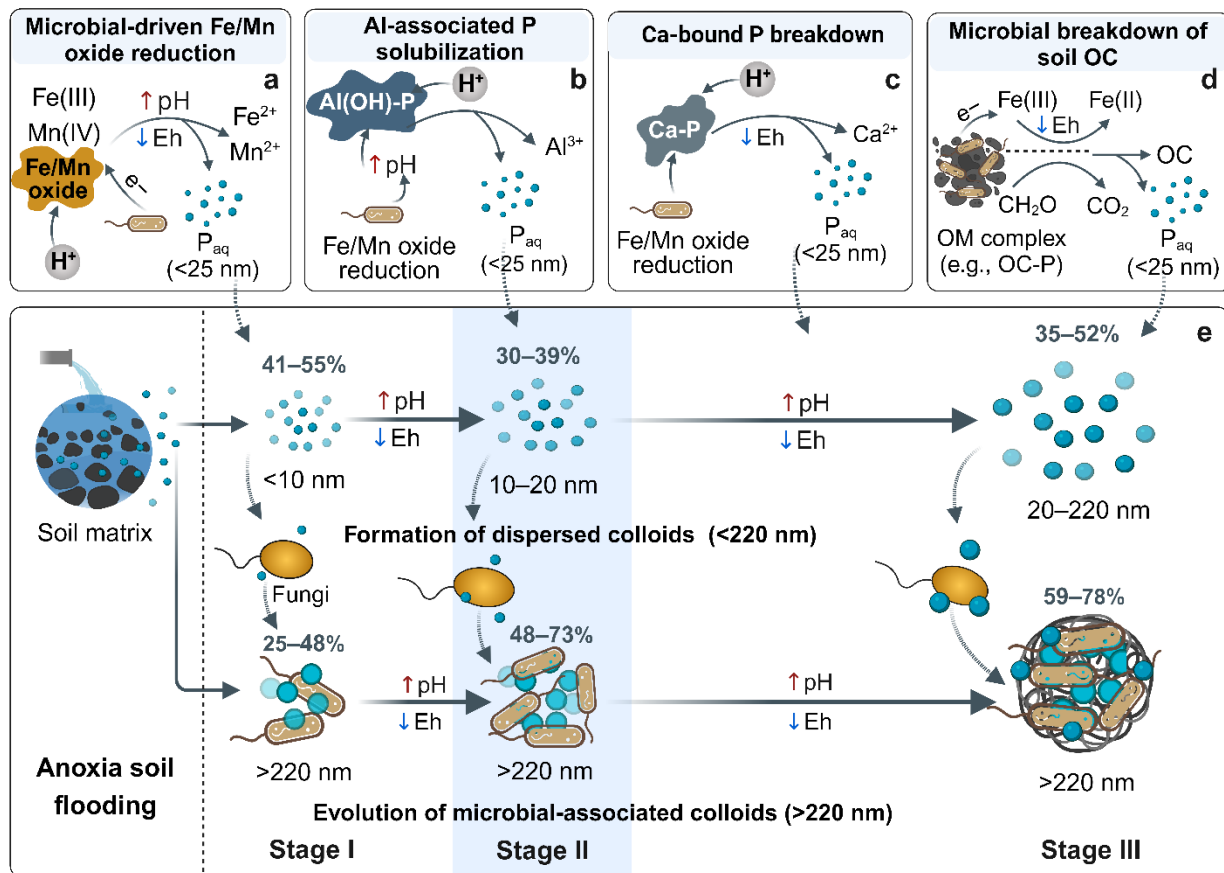


Figure 2. Mechanisms underlying the release of soluble and colloidal P during anoxic flooding. The figure provides a comprehensive view of the mechanisms promoting the release of soluble phosphorus (P_{aq} , $<0.025 \mu m$; a–d) and colloidal phosphorus (P_{coll} ; e) under conditions of anoxic soil flooding.

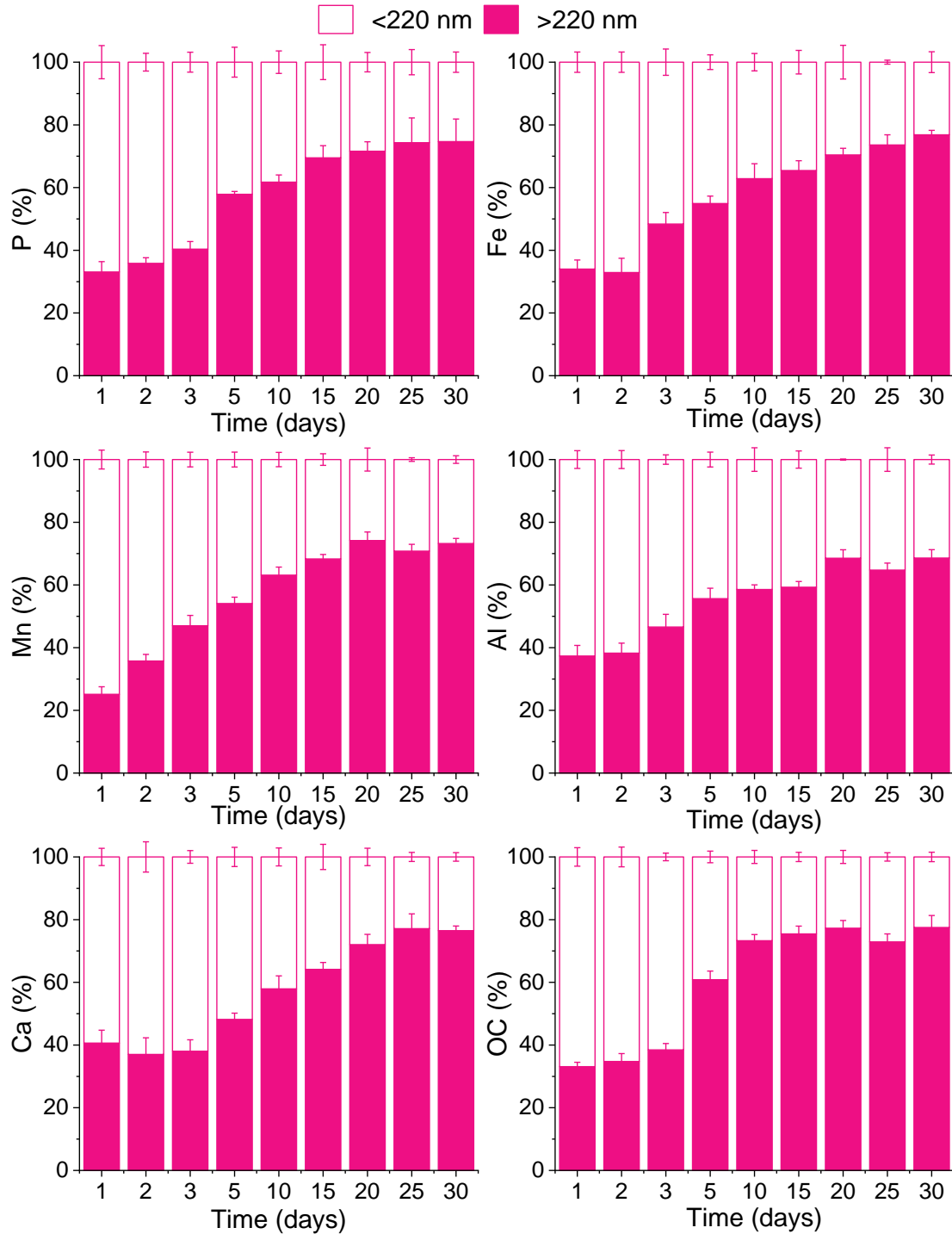


Figure 3. Temporal variability in the elemental composition of microbe-associated and dispersed colloids during 30-day anoxic flooding. The figure presents the percentage concentrations of phosphorus (P), iron (Fe), aluminum (Al), calcium (Ca), manganese (Mn), and organic carbon (OC) in both microbe-associated (>220 nm) and dispersed (<220 nm) colloidal fractions. Values represent means \pm SD ($n = 3$)

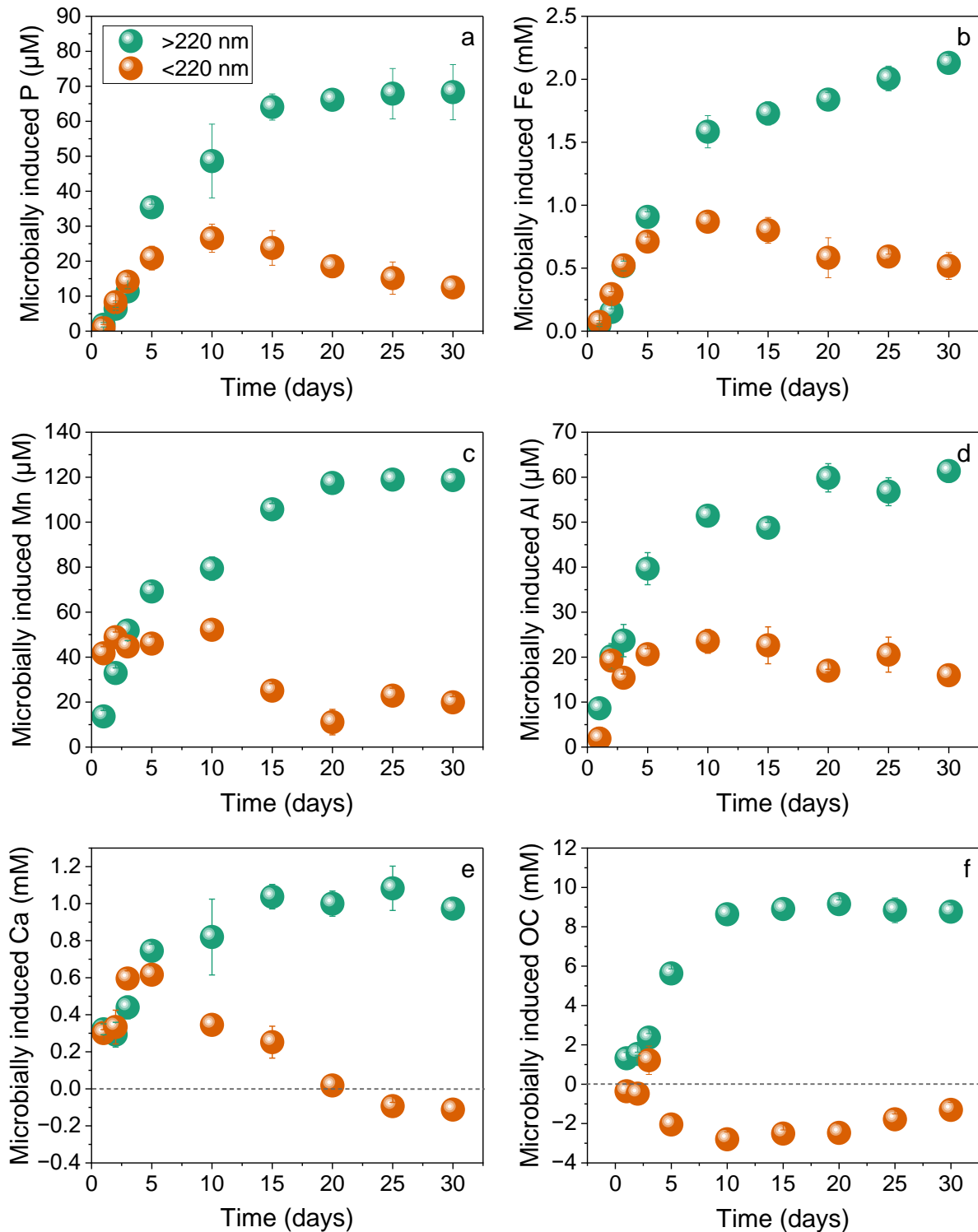


Figure 4. Elemental composition variability of microbe-induced colloids over 30-day anoxic flooding. This depiction assesses the microbial influence on the >220 nm and <220 nm colloidal fractions by determining their net concentrations in anoxic conditions, achieved by subtracting values measured in sterilized settings. Values represent means \pm SD ($n = 3$).

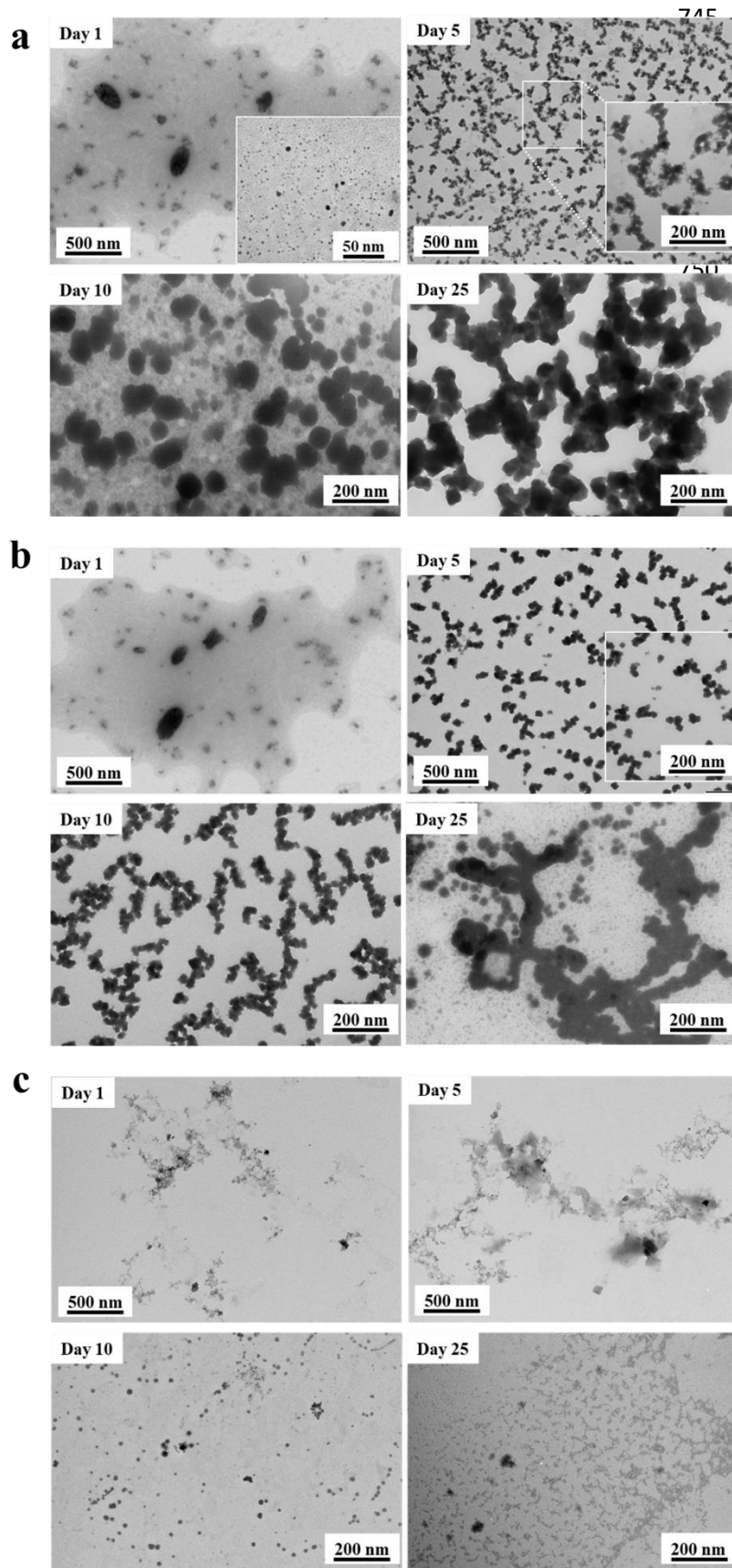


Figure 5. Evolution of colloid morphology in pore water during anoxic treatment (a) in comparison to oxic (b) and sterilized (c) control conditions. TEM observations of colloids generated in pore water at various time points: Day 1, Day 5, Day 10, and Day 25.

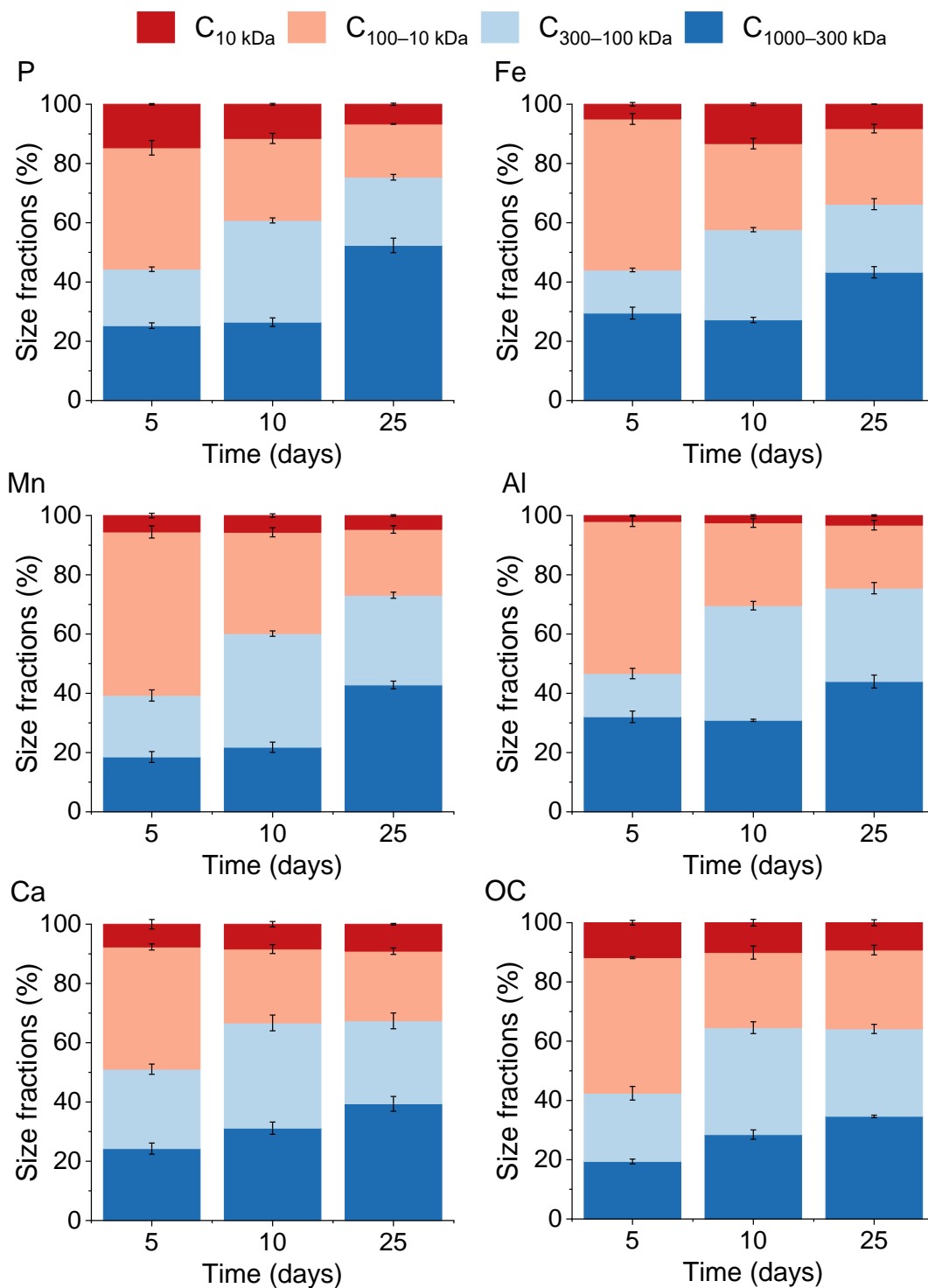


Figure 6. Dynamics of pore-water dispersed colloids under anoxic conditions. Fractionation of freely dispersed colloids of different colloid size ranges in pore water on days 5, 10, and 25. Colloid size ranges were: $<10 \text{ kDa}$ (i.e., $<3 \text{ nm}$), 10 kDa – 100 kDa (~ 3 – 10 nm), 100 kDa – 300 kDa (~ 10 – 20 nm), and 300 kDa – 1000 kDa (~ 20 – 75 nm). Values represent means \pm SD ($n = 3$).

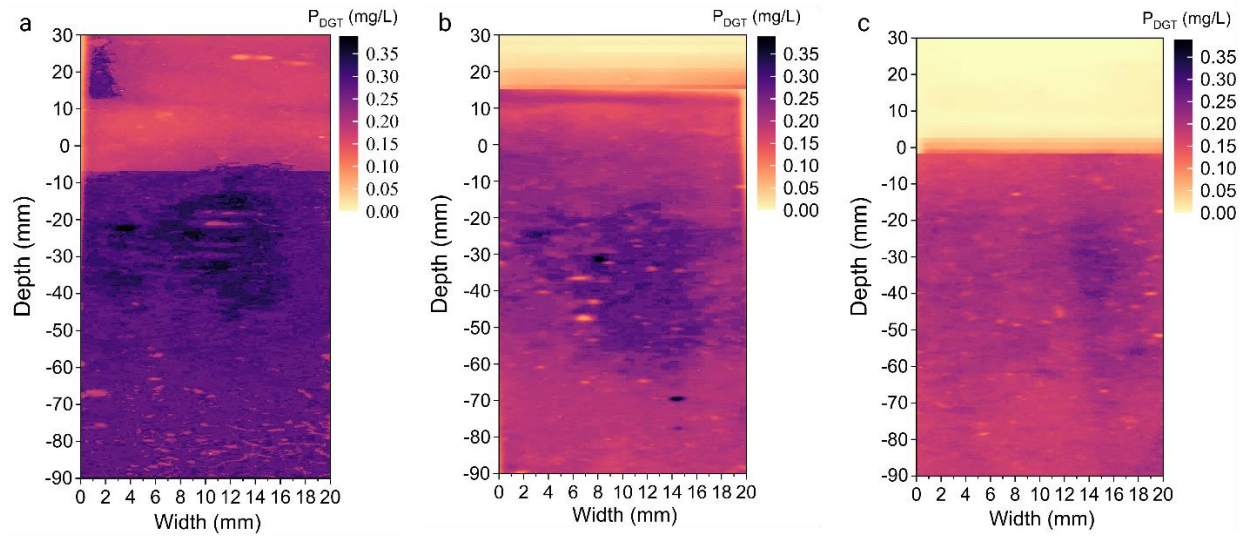


Figure 7. Two-dimensional images of the distribution of DGT-labile P (P_{DGT}) from a secondary DGT strip deployed across the soil-overlying water interface after a 30-flooding incubation under anoxic (a), oxic (b), and sterilized (c) conditions.